NASA TECHNICAL NOTE

NASA TN D-2173

NASA TN D-2173

EVALUATION OF FILAMENT DETERIORATION IN ELECTRON-BOMBARDMENT ION SOURCES

by Nelson L. Milder and William R. Kerslake

Lewis Research Center
Cleveland, Ohio

NATIONAL AERONAUTICS AND SPACE ADMINISTRATION • WASHINGTON, D. C. • MAY 1964

EVALUATION OF FILAMENT DETERIORATION IN ELECTRON-BOMBARDMENT ION SOURCES

By Nelson L. Milder and William R. Kerslake

Lewis Research Center
Cleveland, Ohio

NATIONAL AERONAUTICS AND SPACE ADMINISTRATION

For sale by the Office of Technical Services, Department of Commerce,
Washington, D.C. 20230 -- Price $1.00

EVALUATION OF FILAMENT DETERIORATION IN ELECTRON-BOMBARDMENT ION SOURCES

By Nelson L. Milder and William R. Kerslake

Lewis Research Center

SUMMARY

The attrition of refractory-metal (tantalum) filaments operating in electron-bombardment ion sources using mercury as the propellant was measured from the time variation of filament resistance. Two basic filament geometries, ribbon and wire, were studied in two separate facilities under varying conditions of ion discharge voltage and emission current density.

The results indicate that the primary factors contributing to filament deterioration were the sputtering caused by ion bombardment and the chemical action of residual gases in the facility on the hot filament surface. The presence of mercury vapor had negligible effect on the initial attrition rate in the absence of an ion discharge. A correlation was found among the initial attrition-rate, the ion discharge voltage, and the emission current density.

The maximum filament lifetime attained in this study was 1500 hours. There was evidence that possibly as much as an order of magnitude improvement could be attained for filament operation in ultrahigh vacuum. It appears, however, that such long lifetimes for refractory-metal filaments can only be realized at the expense of propellant utilization efficiency and overall thrustor power efficiency.

INTRODUCTION

Application of electron-bombardment ion thrustors to electric propulsion missions will require systems capable of continuous operation for periods of the order of 10,000 hours. In order to determine whether present ion thrustors meet this requirement, it is necessary to measure the attrition (i.e., the material erosion) characteristics of the various thrustor components. The two components that experience maximum attrition are the ion accelerator electrodes and the electron emitter or filament (ref. 1). Recent studies (refs. 2 and 3) of accelerator electrode erosion have demonstrated the feasibility of constructing electrodes that could meet the 10,000-hour life requirement. The thrustor element that at present determines the upper limit on thrustor life is the filament.

Research electron-bombardment mercury ion thrustors of the Lewis Research Center generally employ refractory metal filaments (ref. 4). Other designs reported in the literature are oxide-impregnated cathodes (ref. 5) and cesium-coated autocathodes (ref. 6). All these cathodes are subjected to continuous

ion bombardment, which may result in the sputtering of filament material. The bombarding ions, which originate in the plasma of the ionization chamber, are accelerated through the plasma sheath surrounding the filament. The degree of filament deterioration resulting from ion bombardment varies with filament type. In the case of the autocathode, for example, the surface coating is constantly replenished by the cesium propellant, and the bombarding cesium ions have energies below the sputtering threshold. The autocathode, however, appears to be useful only for thrustors using cesium propellant.

The purpose of this study was to measure quantitatively the attrition of refractory-metal filaments to determine whether they can be competitive with other types of cathodes. Tantalum and tungsten possess the most favorable thermionic emission characteristics (ref. 7), but tungsten has poor structural characteristics (brittleness) after heating. Consequently, the present study was conducted with tantalum filaments.

The refractory-metal filaments studied herein are subjected to evaporation resulting from the high temperature required for electron emission. Evaporation is thus an additional source of filament attrition. Also, an emitter operating at high temperature for extended periods of time may be subjected to chemical attack (refs. 7 and 8) and surface deformations (ref. 9), which may affect its structural characteristics in such a manner as to induce a localized decrease in filament cross section and subsequent filament destruction.

THEORY

Evaporation rates of tantalum at high temperatures (ref. 10) cannot be used to predict the lifetimes of the ion-thrustor filament because evaporation is not the only mechanism contributing to filament deterioration in the ion discharge chamber of the thrustor. Another contributing process is the sputtering caused by the bombardment of the filament by positive propellant ions formed near the filament and accelerated by the potential difference across the plasma sheath surrounding the filament.

Sputtering of tungsten by mercury ions at bombarding energies less than 300 electron volts has been investigated (ref. 11). The observed dependence of the sputtering yield on ion energy is shown by the solid line in figure 1. The curve has been extrapolated to lower bombarding ion energies (broken portion of the curve) in accordance with the trend of the data for other bombarding materials presented in reference 11. It should be noted that, although the yields presented in figure 1 represent the best available data, they were obtained at temperatures far below those required for appreciable thermionic emission. The available sputtering data for tantalum targets with ion energies in excess of 100 electron volts are in general agreement with similar data for tungsten targets (ref. 12). Consequently, it is presumed that a curve for low-voltage sputtering yield similar to that in figure 1 would also be obtained by using a tantalum target.

If a filament is subjected to a bombarding ion current, the resulting sputtering rate is related to the sputtering yield by the equation

$$\dot{m}_s = j_+ S \tag{1}$$

(All symbols are defined in the appendix.) The magnitude of this current can be estimated from the calculated ion arrival rate per unit area at the cathode sheath:

$$\dot{N}_+ = n_+ \bar{v}_+ \tag{2}$$

It is shown in reference 13 that the ion energy necessary for sheath stability is that corresponding to a mean ion velocity given by

$$\bar{v}_+ = \left(\frac{e\bar{V}_-}{m_+} \right)^{1/2} \tag{3}$$

where the mean electron temperature $e\bar{V}_-$ is about 4 volts (ref. 14). A typical value for ion density is of the order of 10^{12} per cubic centimeter. The mercury ion current density across the sheath is thus approximately

$$j_+ = \dot{N}_+ e = n_+ e \left(\frac{e\bar{V}_-}{m_+} \right)^{1/2} = 3 \times 10^{-2} \text{ amp/sq cm} \tag{4}$$

A comparison between the calculated values of evaporation and sputtering rates will demonstrate the relative magnitudes of the two erosion processes. Consider, for example, a tantalum emitter operating at a temperature of 2400° K. Assume that the sputtering yields of figure 1 are applicable to tantalum and are temperature independent. Figure 2 and table I present three useful temperature-dependent characteristics of tantalum obtained from reference 7. From figure 2 and the density of tantalum (16.6 g/cu cm) the evaporation rate is about 1.1×10^{-5} gram per square centimeter per hour. Evaluation of the sputtering rate requires application of equations (1) and (4) in conjunction with data from figure 2. For a 50-volt ion discharge voltage, the sputtering yield is about 2.6×10^{-3} gram per ampere per hour, and the sputtering rate is about 7.8×10^{-5} gram per square centimeter per hour. Under the prescribed conditions of temperature, ion density, and discharge voltage, the sputtering rate is almost one order of magnitude larger than the evaporation rate.

A relation will be obtained for estimating the lifetime of ribbon filaments in terms of the initial attrition rate. For this purpose it is convenient to define an attrition rate that is proportional to the rate of mass loss per unit cathode surface area:

$$k = -\frac{1}{\rho} \frac{\dot{M}}{2Lw_0} \tag{5}$$

The filament mass is given by

$$M = \rho L l w_0 \tag{6}$$

and the filament resistance is given by

$$R = \frac{rL}{lw_0} \tag{7}$$

For constant values of ρ, r, L, and w_0, the attrition rate becomes

$$k = \frac{l}{2}\frac{\dot{R}}{R} \tag{8}$$

A similar procedure can be used to show that for the wire filaments of diameter ϵ the attrition rate is

$$k = \frac{\epsilon}{4}\frac{\dot{R}}{R} \tag{9}$$

An estimation of filament lifetime in terms of the initial attrition rate and the filament thickness (l_0 or ϵ_0) can be effected in the following manner.

If mass is lost uniformly from the filament surface area at a constant rate,

$$\dot{M} = -\alpha \tag{10}$$

where α is a constant. Integration and substitution of equation (6) into the resulting equation yield

$$lw_0 = l_0 w_0 - \frac{\alpha}{\rho L} t \tag{11}$$

where l_0 is the initial filament thickness and ρ, L, and w_0 are assumed constant.

Differentiation of equation (7) with respect to time and substitution of equation (11) into the result give the relation

$$R = \frac{R_0}{1 - \beta t} \tag{12}$$

where $\beta = \alpha/\rho L l_0 w_0$ is constant. An identical expression results for wire filaments if the denominator of equation (7) is replaced by the cross-sectional area of the wire. Differentiating equation (12) and substituting the result into equations (8) and (9) give the relations

$$\beta = \frac{2k}{l + 2kt} \tag{13}$$

for ribbon filaments and

$$\beta = \frac{4k}{\epsilon + 4kt} \tag{14}$$

for wire filaments. Noting that $k = k_0$ at $t = 0$ and employing the fact that

β is a constant result in the following equations:

$$l + 2kt = l_0 \frac{k}{k_0} \tag{15}$$

and

$$\epsilon + 4kt = \epsilon_0 \frac{k}{k_0} \tag{16}$$

A calculation of filament lifetime can be effected by allowing the filament thickness l or diameter ϵ to vanish, which corresponds to complete conversion of the filament into sublimated material. The conversion process is assumed to proceed uniformly along the entire filament length.

Thus, the lifetimes are

$$t_L = \frac{l_0}{2k_0} \tag{17}$$

for ribbon filaments and

$$t_L = \frac{\epsilon_0}{4k_0} \tag{18}$$

for wire filaments.

The β parameter of equation (14) can be written with the aid of equations (15) and (16) in terms of the attrition rate at time $t = 0$. The resulting expressions for resistance become

$$R = \frac{R_0}{1 - \frac{2k_0}{l_0} t} \tag{19}$$

for ribbon filaments and

$$R = \frac{R_0}{1 - \frac{4k_0}{\epsilon_0} t} \tag{20}$$

for wire filaments.

APPARATUS

The present investigation of filament attrition in electron-bombardment ion sources was undertaken in two separate vacuum facilities. Short-run experiments

were performed in the 5-foot-diameter, 16-foot-long vacuum tank described in reference 15. These tests employed small-diameter wire filaments. Test conditions simulated those in an actual thrustor with the exception that, because of the small diameter of the filament, the total emission current was low. The emission current density, however, corresponded to that of an actual thrustor.

Since the vacuum-tank studies measured primarily gross effects, more detailed and longer duration studies of filament characteristics under controlled conditions were performed in a standard 20-inch-diameter bell-jar apparatus (fig. 3).

Vacuum-Tank Installation

A 10-centimeter-diameter electron-bombardment ion thrustor (ref. 4) was used to determine the attrition rates of tantalum wire filaments mounted coaxially with the thrustor axis. Thrustor power supplies (ref. 3) were located near the vacuum tank. Filament heating power was furnished by a 60-cycle supply. The alternating voltage and current were measured near the filament supports in order to avoid including lead losses. The meter readings were accurate to 3 percent of full scale. The time variation of filament resistance was determined from the variation of the filament heating current and voltage, which were adjusted to maintain a constant emission current. Mercury was vaporized in a steam-heated boiler and entered the ionization chamber through a flow-calibrated orifice with a 0.05-inch diameter. The equivalent neutral current, defined as the current obtained by assuming each mercury atom entering the chamber to be singly ionized, was 80 milliamperes (0.6 g/hr). Pressure in the vacuum tank was maintained at 10^{-5} millimeter of mercury during thrustor operation. The filaments studied in this facility were small-diameter tantalum wires (data presented in table II). Filament supports were constructed from 0.318-centimeter-diameter stainless-steel rods. The ratio of support to filament cross-sectional area was thus about 200 to 1. This fact, together with the fact that the operating temperature of the supports was nearly 2000° K less than that of the filament, indicated that the support resistance was negligible in comparison with the filament resistance.

Bell-Jar Installation

A 7.5-centimeter-diameter ion source and a filament evaporation test apparatus were operated concurrently in a 20-inch-diameter bell jar (fig. 3), which was supported by a 20-inch-inside-diameter spool piece 12 inches high. This structure contained electrical, steam, and vacuum gage ports, as shown in figure 3. The experimental test apparatus was mounted to the top flange of the spool piece.

Bell-jar pressures ranging from 3×10^{-7} to 9×10^{-6} millimeter of mercury were provided by a 6-inch oil-diffusion pump equipped with a liquid-nitrogen cold trap.

The electron-bombardment ion source was constructed of stainless steel and

is shown in figure 4 with the screen grid removed.

Figure 5 is a schematic of the complete ion-source installation. The general design of this source was similar to that of the ion thrustor described in reference 3. Mercury was vaporized by means of a steam boiler. Calibrated orifices were used to regulate the mercury flow. The propellant vapor entered the ionization chamber through the concentric annular distributor plates. The cylindrical anode was 7.5 centimeters in diameter and 5.7 centimeters in length. Filament supports were mounted in a boron nitride slug positioned coaxially with the source.

At the downstream end of the ionization chamber, a 0.08-centimeter-thick stainless-steel screen with a 50 percent open area provided an ion and vapor exit. The screen contained a 2.5-centimeter-diameter hole for optical pyrometer temperature measurements of the filament. The exhausted ions and vapors were condensed on a liquid-nitrogen-cooled stainless-steel can, 16 centimeters in diameter and 20 centimeters in length. This cold trap was mounted coaxially with the ion source. The rear of the trap was provided with a 3-centimeter-diameter hole, again for the purpose of enabling visual observation of the filament. A movable shield was used to cover this hole when temperature measurements were not being made. This shield was necessary because mercury vapor condensation and deposits of sputtered particles on the bell-jar wall would have acted as an optical filter and thus resulted in erroneous readings of filament temperature.

An approximately axial magnetic field required for containment of electrons in the ion chamber was provided by two coils wound about each end of the chamber.

The circuit diagram for the ion source is also shown schematically in figure 5. The filament was heated by a 60-cycle alternating-current power supply. Separate potentiometer leads connected the filament supports to the instrumentation panel. Filament heating voltage and current were monitored by meters accurate to 1 percent of full scale. Other meters used in this investigation were accurate to 3 percent of full scale. The anode was maintained at the desired voltage by a regulated direct-current power supply. The filament emmission was measured by a ground return meter.

An auxiliary filament evaporation test apparatus (fig. 3) was operated simultaneously with the ion source. This unit consisted of a 14-centimeter-diameter stainless-steel can enclosing a filament identical with the ion-source filament. A boron nitride block was used to support the filament leads. A cylindrical can served to shield the observer against the intense incandescence of the heated filament. The filament used in this assembly was heated and was monitored in a manner similar to that for the ion source.

PROCEDURE

Vacuum-Tank Installation

The experiments performed in the vacuum tank were intended to provide a

measure of the time rate of change of filament resistance in a reasonably short period of run time. Fourteen filaments were used for runs performed under the various conditions of discharge voltage and emission current given in table II. A net ion accelerating potential of 2500 volts was maintained for all tests. Because of the low emission currents employed, propellant utilization, defined as the ratio of beam current to equivalent neutral current, ranged from 8 to 12 percent. The ratio of emission to beam current was in agreement with the previously reported ratio of about 10 to 1 (table III of ref. 2). Filament heating power ranged from approximately 14 to 19 watts for the three emission currents used.

Each test continued for a period of 16 hours after an initial 1/2 hour of operation for thrustor stabilization. The time variation in filament resistance was determined from the measured values of filament heating current and voltage.

Variation in filament temperature was assumed negligible over the 16-hour run time. Any temperature variation would be due to variation in emitting surface area, since the emission current was held constant.

Bell-Jar Installation

Operation of the ion source in the bell-jar experiments consisted of presetting the mercury flow rate, the ion discharge voltage, and the magnetic field. The filament heating current was adjusted to maintain a constant emission current. In general, the source was operated continuously until filament burnout. Some tests were terminated before burnout when only the initial attrition rate was desired.

The ion-source magnetic field was varied in order to ascertain the effect of magnetic field on the discharge current. Optimization of this current occurred for an axially diverging field of 32 gauss at the upstream (or distributor) end of the source and 23 gauss at the downstream (or screen) end.

Ribbon filaments were primarily investigated in this facility, although some tests were performed with wire filaments (data presented in table III (a)). The ribbon filaments were formed from tantalum sheets of different thicknesses. The two effective emitting surfaces of the filaments were, in general, 0.36 centimeter wide and 5.1 centimeters long (fig. 5). The enlarged area at the center of the filament was required to prevent local overheating, since it has been found that its exclusion results in premature burnout at the bend. The effective increase in emitting surface due to this enlarged area was approximately compensated for by the temperature decrease, and the emission current did not essentially differ from that which would have been obtained from a truly rectangular geometry.

Filament power ranged from 100 to 200 watts depending on the emission current used and the initial attrition rate. Filament heating, voltage, current, and temperature were observed at 1/2-hour intervals. For tests exceeding 250 hours, it was necessary to interrupt the run in order to replenish the mercury supply.

The temperature of the filament was determined in two ways - from the optical-pyrometer measurements and from the graph of emission current density against temperature. The temperatures presented in tables III and IV were obtained by the latter method. The temperature values obtained from the pyrometer readings were somewhat lower than those obtained from the graph. This probably was due to slight coating of the bell-jar inner surface by mercury condensation or sputtered particles. Filament attrition rates were determined from the increase in resistance with time, in the manner described previously.

The filaments studied in the evaporation test apparatus (table IV) were elevated to temperatures comparable to those in the ion source and were held at constant heating power. The filament environment was free of mercury vapor. Data obtained from these studies were compared with data obtained from the ion source.

RESULTS

The observed resistance variation with time was in good agreement with the theoretically predicted variation, as can be seen from figures 6 and 7. Figure 6 compares the theoretical curve for 0.005-centimeter-thick ribbon filaments with the observed variation of three such filaments. Since the actual lifetime of the three filaments ranged from 17 to 68 hours, the time scale of figure 6 is normalized.

A 0.025-centimeter-diameter tantalum wire was used to determine the validity of the theory in the case of wire filaments. The results of the comparison are presented in figure 7. Again the agreement is good, which implies that the assumption of constant mass loss is valid. The variation of resistance with time, shown in figure 8, was obtained from actual measurements on ribbon filaments operating in the bell-jar ion source and had the same general form independent of the total length of run. Of particular interest, however, are the discontinuities or steps labeled 1 to 6 in figure 8(c). These steps correspond to times at which the run was interrupted in order to replenish the propellant (mercury) supply. At such times the filament was allowed to cool to room temperature, after which the liquid-nitrogen flow to the cold trap of the diffusion pump was terminated and the bell jar raised to atmospheric pressure. The effect of this filament cooling and pressure elevation is a step increase in filament attrition with an accompanying rise in filament resistance. Since ambient-pressure changes were a possible reason for the step increases in attrition shown in figure 8, the effect of pressure was determined in separate tests.

The ratio of the observed initial attrition rate to the literature value of evaporation rate (fig. 2) in vacuum at a particular temperature is presented in figure 9 as a function of the ion-gage reading of the mean bell-jar pressure. (The temperature varied from point to point - the overall temperature range being about 2200° to 2500° K.) The pressure varied from the highest value at the beginning of a run to the lowest value at the end of the run. A bar shown with each data point represents the range of this variation. It can be seen from the figure that the observed attrition rates exceeded the evaporation rates at pressures of the order of 10^{-6} millimeter of mercury. At bell-jar pressures of the

order of 10^{-7} millimeter of mercury, the ratio of attrition rate to evaporation rate was observed to approach unity.

The effect of mercury vapor on filament attrition in both the presence and the absence of a discharge is presented in figure 10. The temperature of the filaments operated in the absence of a discharge was about 2330° K. As can be seen from the figure, filament attrition in the absence of an ion discharge is independent of the neutral mercury flow rate. In the presence of a discharge, however, there is an increase in filament attrition. This increase in filament attrition decreases with increasing flow rate. This is believed to be caused by a decrease in the filament temperature with an increase in the mercury flow. The initial attrition rate apparently levels off to a constant value as the flow rate approaches 0.3 equivalent ampere. The difference between this value of the attrition rate and that observed under conditions of no discharge is a measure of the sputtering rate as a function of temperature at an ion energy of approximately 50 electron volts.

Initial attrition rates were determined under conditions of varying emission current density and discharge voltage for both ribbon and wire filaments. The results of these measurements are presented in figure 11 for ribbon filaments with a 0.005-centimeter thickness. The curves indicate an exponential increase in initial attrition rate with discharge voltage at three emission current densities and a linear dependence of the initial attrition rate on emission current density. The fact that only a linear dependence was observed implies that evaporation was probably negligible at the 2400° K operating temperature and that the number of impinging ions is proportional to the number of emitted electrons.

Figure 12 presents the initial attrition rates of wire filaments as a function of ion discharge voltage. The dependence differs somewhat from that observed for ribbon filaments. The initial attrition rate decreased with increasing discharge voltages less than 40 volts, while a linear increase in the initial attrition rate was noted for voltages greater than 40 volts. No appreciable dependence on emission current density was observed.

A characteristic of filaments that were operated to burnout was that the final resistance as measured just prior to burnout was generally greater than that predicted from the theory. This is illustrated in figure 13. The solid points lying to the right of the theoretical 45° line represent runs in which burnout occurred and are plotted for 0.005-centimeter-thick ribbon filaments without regard to operating conditions. The open points represent runs terminated substantially prior to burnout and follow the 45° line quite well. The solid points, therefore, indicate a marked rise in filament resistance just prior to burnout without an accompanying rise in mass loss.

Visual observation of filaments before and after operation revealed the formation of grain boundaries and structural deformations, as shown in figure 14. These photomicrographs were obtained for a ribbon filament operated to burnout. The coarse appearance of the surface, due to the formation of these grain boundaries (left inset), is presumably the result of ion bombardment. The center inset shows the marked structural deformation caused by local hot spots. Phenomena

such as grain boundary formations and hot spots contribute to the deviation of actual filament lifetimes from the theoretically predicted lifetimes of equations (17) and (18).

For example, a tantalum wire filament 0.025 centimeter in diameter was found experimentally to have an initial attrition rate of approximately 2.5×10^{-5} centimeter per hour. Inserting these values into equation (18) yields a calculated lifetime of about 250 hours. The observed lifetime was 190 hours.

In practice it is necessary to introduce a burnout factor in order to obtain a more accurate estimate of filament lifetimes. This factor accounts for the fact that filament failure occurs before complete attrition and can be determined experimentally from the ratio between observed and calculated lifetimes, the latter quantity being obtained from equation (17) or (18). The resulting lifetime equations will thus have the form

$$t_L = f_r \frac{l_0}{2k_0} \tag{21}$$

for ribbon filaments, and

$$t_L = f_w \frac{\epsilon_0}{4k_0} \tag{22}$$

for wire filaments.

The values of f_r and f_w obtained in this investigation for tantalum filaments are presented in the follow table:

Number of samples	Emission current density, j_E, amp/sq cm	Initial wire filament diameter, ϵ_0, cm	Wire filament burnout factor, f_w	Initial ribbon filament thickness, l_0, cm	Ribbon filament burnout factor, f_r
1	0.42	0.025	0.67	-----	---------
1	.41	.051	.24	-----	---------
1	.95	-----	----	0.005	0.50
10	.55	-----	----	.005	0.50±0.04
5	.27	-----	----	.005	0.60±0.07
2	.55	-----	----	.025	0.28

The burnout factors did not vary appreciably with the discharge voltage over the range employed (25 to 50 v). The results indicate a decrease in the burnout factor with increasing filament thickness; no regular variation of these factors with j_E was observed. The lower values of the burnout factor were obtained for the lower initial attrition rates.

DISCUSSION OF RESULTS

Comparison Between Bell-Jar Ion-Source and Thrustor Operation

Throughout this investigation it was assumed that the bell-jar ion-source operation closely simulated thrustor operation in the large vacuum facility. The basis for this assumption lies in the observed agreement with theory in both cases. The theory employed here assumes only that the rate of mass loss is constant. The major difference between the two operations is the absence of a large ion accelerating voltage for the bell-jar ion source. The presence of this voltage improves the ion-extraction efficiency so that any discrepancy between the results of bell-jar and tank operation might appear as a lower initial filament attrition rate for thrustors. The measured initial attrition rates in both operations usually agreed within a factor of 2, and thus, no discrepancy was evident within the accuracy of the experiment.

Effect of Filament Environment

In the absence of a discharge, filament attrition appears to be independent of the neutral mercury density. The difference between the measured attrition rate and the literature values of evaporation rates (fig. 9) is probably the result of the chemical action of residual bell-jar gases at the hot filament surface. Tantalum is known to have a high affinity for oxygen and nitrogen (ref. 7). One possible result is the formation of an oxide with a vapor pressure exceeding that of pure tantalum at the operating temperature.

Factors Influencing Sputtering Rate

The data presented in figure 10 show that the initial attrition rate increases with decreasing neutral mercury flow rate in the presence of a discharge. At low flow rates, or low mercury densities, it was necessary to increase the filament temperature in order to maintain a constant emission current. The reason for this is that at the lower ion densities (the ion density is assumed proportional to the neutral mercury density) an increased net negative space charge is established because of the increased sheath dimensions (ref. 16). This space charge tends to repel emitted electrons. If the filament temperature is increased, the number of electrons with sufficient energy to penetrate the space charge is increased, and the given emission current can be maintained. The larger values of the initial attrition rate at the lower flow rates may be an indication of increased sputtering at the higher filament temperature. The lack of sputtering data for material temperatures of the order of 2000° K prohibits definite conclusions on this point.

In the THEORY section of this paper it was shown that, based on equation (4) and the data of figure 1, a sputtering rate of about 7.8×10^{-5} gram per square centimeter per hour, or 4.7×10^{-6} centimeter per hour, at a 50-volt ion discharge is predicted. In the present study the measured sputtering rates were larger

than the calculated value. This can be readily seen with the aid of figure 10. The difference between no-discharge initial attrition rates and with-discharge rates at a neutral flow of about 0.3 equivalent ampere was stated earlier to be a measure of the sputtering rate. For an emission current density of 0.28 ampere per square centimeter the sputtering rate is about 1.3×10^{-5} centimeter per hour, while for an emission current density of 0.55 ampere per square centimeter it is about 3×10^{-5} centimeter per hour.

The initial attrition rate of wire filaments was a decreasing function of ion discharge voltage in the range 25 to 40 volts (fig. 12). As in the case of ribbon filaments, where it was necessary to increase the filament temperature in order to maintain a constant emission current at low neutral flow rates, it was also necessary in this case to raise the filament temperature in order to keep a constant emission current. At the lower ion discharge voltages, the voltage gradient, or electric force, is small, and a net negative space charge results. The effect is thus analogous to that described for ribbon filaments and low propellant flow rates.

Surface Deformations

The occurrence of high temperature and sputtering-induced surface deformations may also contribute to filament deterioration. The left inset of figure 14 shows the formation of grain boundaries. These boundaries would be etched preferentially by ion bombardment, and localized filament deterioration would result. A further indication of local structural failure is the marked increase in filament resistance near burnout without a corresponding increase in mass loss (fig. 8).

Dependence of Initial Attrition Rate on Ion Discharge Voltage and Emission Current

Empirical relations for the initial attrition rate valid over limited ranges of operating conditions can be obtained for ribbon filaments with the aid of figure 11 and for wire filaments with the aid of figure 12. The resulting relation for ribbon filaments, which is valid for discharge voltages of the order of 50 volts and emission current densities ranging from 0.28 to 0.55 ampere per square centimeter, is

$$k_0 \sim 1.2\times10^{-11}\,\Delta V_I^4 j_E \tag{23}$$

This relation fits the data to within a maximum error of less than 10 percent at a 50-volt discharge. The corresponding relation for wire filaments, which is based on figure 13 for discharge voltages ranging from 40 to 70 volts with the emission current density ranging from 0.42 to 0.84 ampere per square centimeter, is

$$k_0 \sim 2.3\times10^{-6}\,\Delta V_I \tag{24}$$

The lack of dependence of the initial attrition rate on the emission current density may be due to the filament geometry, although this result is not well understood.

Comparison of Two Filament Geometries Studied

Since ribbon filaments possess a large emitting surface area with a small cross-sectional area, the emission current per watt of heating power is more favorable than for the wire geometry. The sharp edges associated with the ribbon geometry are subjected to intense ion bombardment and thus sputtering, however, because of the large electric-field strengths at these edges.

The wire geometry has no sharp edges and is thus not subject to these high localized field strengths (precluding grain boundary formation at the surface). The disadvantage, however, of lower emission current per watt of heating power tends to outweigh the advantage of no sharp edges, since it reduces thrustor efficiency.

Lifetime Capabilities of Filaments

The maximum filament lifetime attained in this program was about 1500 hours of testing time. To attain this lifetime, however, it was necessary to operate at a low emission current density and a low ion discharge voltage, which correspond to a low overall power efficiency and a low propellant utilization efficiency. This lifetime capability could conceivably be as much as an order of magnitude larger for thrustors operating in the ultrahigh vacuum of space, where the effect of atmospheric gases on filament attrition would be negligible. In this case attrition would be due only to sputtering by propellant ions.

In general, the best performance characteristics were obtained for the higher mercury flow rates; that is, increasing the propellant flow rate from about 0.16 to 0.3 ampere increased filament life by about 10 percent. It is possible that the increased neutral mercury density in the ion chamber shields the cathode from ion bombardment, but this explanation is only a conjecture at this time.

SUMMARY OF RESULTS

The following results were obtained from an investigation of the attrition of tantalum filaments operating in electron-bombardment ion sources using mercury as the propellant:

1. Tantalum filaments operating in an ion discharge lost mass at an approximately constant rate until just prior to burnout, at which time a localized rapid structural deterioration occurred.

2. Filament attrition was sensitive to the presence of residual bell-jar gases, which may have included hydrocarbons, nitrogen, oxygen, and possibly

water vapor.

3. In the absence of an ion discharge, the initial attrition rate was insensitive to the neutral mercury flow rate. In the presence of a discharge, a greater dependence of initial attrition rates on neutral flow rates was observed.

4. The major factor contributing to filament deterioration was sputtering resulting from ion bombardment. The sputtering rate exhibited an exponential dependence on discharge voltage for ribbon filaments. A linear dependence on discharge voltage was observed for small-diameter wire filaments.

5. The maximum lifetime of filaments attained in this investigation was 1500 hours, but this value could conceivably be increased by as much as an order of magnitude for thrustor operation in ultrahigh vacuum. The results indicate, however, that such long lifetimes of refractory-metal filaments can be attained only at low values of propellant utilization efficiency and overall thrustor power efficiency. Consequently, their application to space missions appears to be limited. For long-duration missions other types of filaments, such as oxide-coated cathodes and (for cesium) autocathodes, may show more promise.

Lewis Research Center
National Aeronautics and Space Administration
Cleveland, Ohio, December 3, 1963

APPENDIX - SYMBOLS

e	electronic charge, 1.6×10^{-19} coulomb
f_r	burnout factor for ribbon filaments, dimensionless
f_w	burnout factor for wire filaments, dimensionless
J_E	total emission current, amp
J_F	filament heating current, amp
J_I	anode current, amp
J_O	mercury flow, ma
j_E	emission current density, amp/sq cm
j_+	positive ion current density, amp/sq cm
k	attrition rate, cm/hr
k_O	initial attrition rate, cm/hr
L	filament length, cm
l	ribbon filament thickness, cm
l_O	initial thickness of ribbon filament, cm
ΔM	change in mass, $M_O - M_f$, g
M_f	final mass of filament, g
M_O	initial mass of filament, g
$\dot{M}$	rate of filament mass loss, g/hr
m_+	ion mass, g
$\dot{m}_s$	sputtering rate, g/(sq cm)(hr)
$\dot{N}_+$	ion arrival rate, $(cm^{-2})(sec^{-1})$
n_+	ion density, cm^{-3}
R	filament resistance, ohms
ΔR	change in resistance, $R_f - R_O$, ohms
$\dot{R}$	rate of change of filament resistance, ohms/hr

R_f filament resistance at burnout, ohms

R_0 initial filament resistance, ohms

r resistivity, (ohms)(cm)

S sputtering yield, g/(amp)(hr)

T_{av} average temperature, ^{o}K

t time, hr

t_L filament lifetime, hr

V_F filament heating voltage, v

ΔV_I ion discharge voltage, v

$\overline{V}_-$ plasma potential, v

$\overline{v}_+$ mean ion velocity, cm/sec

w_0 filament width, cm

α constant, g/hr

β constant, hr^{-1}

ϵ wire filament diameter, cm

ϵ_0 initial wire filament diameter, cm

ρ filament mass density, g/cu cm

REFERENCES

1. Mickelsen, William R., and Kaufman, Harold R.: Status of Electrostatic Thrustors for Space Propulsion. NASA TN-2172, 1964.

2. Kerslake, William R.: Accelerator Grid Tests on an Electron-Bombardment Ion Rocket. NASA TN D-1168, 1962.

3. Kerslake, William R.: Charge-Exchange Effects on the Accelerator Impingement of an Electron-Bombardment Ion Rocket. NASA TN D-1657, 1963.

4. Reader, Paul R.: Investigation of a 10-Centimeter-Diameter Electron-Bombardment Ion Rocket. NASA TN D-1163, 1962.

5. Sirois, William: Cathode Development Studies for Arc and Bombardment-Type Ion Engines. Rep. 34TR-073, NASA Contract NAS8-2513, Apr. 13, 1963. (Available from NASA (Attn: AFSS-A), Washington, D.C.)

6. Taylor, Lawnie H.: Ionizer Development and Surface Physics Studies. EOS Rep. 1660/1-IR-1, Electro-Optical Systems, Inc., Dec. 1962.

7. Kohl, Walter H.: Materials and Techniques for Electron Tubes. Reinhold Pub. Corp., 1960.

8. Majors, H. Jr., Wallace, R. H., Webster, R. T., and Wendell, G. E.: Materials Handbook. Parts 4 and 7. Properties of Tantalum, CRD-A19-27, California Research and Development Co., April 1953.

9. Gilbert, A., Hull, D., Owen, W. S., and Reid, C. N.: The Yield of Polycrystalline Tantalum. Jour. of the Less-Common Metals, vol. 4, no. 5, Oct. 1962, pp. 399-408.

10. Langmuir, D. B., and Malter, L.: Rate of Evaporation of Tantalum. Phys. Rev., vol. 55, 1939, pp. 748-749.

11. Stuart, R. V., and Wehner, G. K.: Sputtering Yields at Very Low Bombarding Ion Energies. Jour. Appl. Phys., vol. 33, no. 7, July 1962, pp. 2345-2352.

12. Wehner, G. K., and Rosenberg, D.: Mercury Ion Beam Sputtering of Metals at Energies of 4 to 15 Kev. Jour. Appl. Phys., vol. 32, no. 5, May 1961, pp. 887-890.

13. Guthrie, A., and Wakerling, R. K., eds.: The Characteristics of Electrical Discharges in Magnetic Fields. McGraw-Hill Book Co., Inc., 1949, pp. 87-91.

14. Kaufman, Harold R.: The Neutralization of Ion-Rocket Beams. NASA TN D-1055, 1961.

15. Keller, Thomas A.: NASA Electric Rocket Test Facilities. Seventh Nat. Symposium on Vacuum Tech. Trans., Pergamon Press, 1960, pp. 161-167.

16. Spitzer, Lyman: Physics of Fully Ionized Gases. Interscience Pub., Inc., 1956.

TABLE I. - THERMAL CHARACTERISTICS

OF TANTALUM

[Data from ref. 7.]

Emission current density, j_E, amp/sq cm	Filament temperature, °K	Radiated power density, w/sq cm	Evaporation rate, cm/hr
0.0068	2000	21.6	3.5×10^{-10}
.0226	2100	27.1	2.9×10^{-9}
.0675	2200	34.2	1.9×10^{-8}
.192	2300	42.2	1.2×10^{-7}
.495	2400	51.3	6.6×10^{-7}
1.196	2500	62.4	2.9×10^{-6}
2.71	2600	75.4	1.24×10^{-5}
5.85	2700	89.9	4.40×10^{-5}

TABLE II. - EXPERIMENTAL DATA FOR ION-SOURCE OPERATION IN VACUUM TANK

[Filament, tantalum wires, 0.025 cm diam., 3.02 cm length; mercury flow, 80 ma; tank pressure, 10^{-5} mm Hg; net ion accelerating voltage, 2500 v; length of run, 16 hr.]

Emission current density, j_E, amp/sq cm	Filament temperature, °K	Ion discharge voltage, ΔV_I, v	Radiated power density, w/sq cm	Initial attrition rate, k_0, cm/hr
0.42	2380	30	60	1.6×10^{-5}
		40	60	1.2
		50	58	4.2
		70	56	7.9
0.63	2420	25	67	4.6×10^{-5}
		30	63	3.2
		40	61	2.0
		50	61	4.1
		70	58	8.9
0.84	2450	25	78	4.3×10^{-5}
		30	71	3.3
		40	69	1.1
		50	65	4.0
		70	63	8.3

TABLE III. - EXPERIMENTAL DATA FOR ION-SOURCE OPERATION IN BELL-JAR APPARATUS

(a) With discharge

Filament material and geometry	Filament dimensions, cm	Emission current density, j_E, amp/sq cm	Ion discharge voltage, ΔV_I, v	Mercury flow rate, ma	Length of run, hr	Initial attrition rate, k_o, cm/hr	Filament temperature, °K	Radiated power density, w/sq cm	Bell-jar pressure, mm Hg
Tantalum wire	0.025 diam. × 3.0	0.42	50	80	[a]190	2.3×10^{-5}	2380	54	0.7×10^{-6}
	0.051 diam. × 3.06	.41	50	80	[a]400	.5	2380	56	.5
Tantalum ribbon	5.1 × 0.36 × 0.005	1.36	50	160	63	12.0×10^{-5}	2510	62	2.0×10^{-6}
90%-tantalum - 10%-tungsten ribbon	5.1 × 0.36 × 0.005	.95	50	160	[a]18	7.7	2470	57	.9
Tantalum ribbon	5.1 × 0.36 × 0.005	0.95	50	160	[a]125	7.0×10^{-5}	2470	75	1.3×10^{-6}
		0.55	50	160	[a]30	3.7×10^{-5}	2410	48	3.0×10^{-6}
			50	↓	[a]35.5	3.8	↓	49	1.0
			50		25	3.7		48	2.5
			30		153	.4		47	1.0
			25		111	.19		50	.8
			50	320	22	3.4		45	1.3
			50	80	[a]17	7.4		49	2.5
		0.28	50	160	[a]68	2.2×10^{-5}	2330	40	2.6×10^{-6}
			40	↓	130	.8	↓	40	.9
			35		[a]190	.6		41	.4
			30		[a]230	.24		38	.7
			25		79	.05		43	.7
			50	320	[a]74.5	1.8		41	3.0
			50	80	[a]29.5	4.6		42	2.7
		0.14	50	160	113	1.3×10^{-5}	2260	38	1.0×10^{-6}
			30	160	324	.06	2260	38	1.6
			25	160	[a]1478	.05	2260	39	.6
	5.1 × 0.36 × 0.013	0.55	50	160	[a]79	3.0×10^{-5}	2410	59	1.0×10^{-6}
	5.1 × 0.23 × 0.025	.54	↓	↓	[a]171	2.6	↓	63	.8
	5.1 × 0.33 × 0.025	.55			[a]135	2.6		64	1.4
	5.1 × 0.33 × 0.025	.55			[a]155	2.3		46	1.0

[a]Burnout.

TABLE III. - Concluded. EXPERIMENTAL DATA FOR ION-SOURCE OPERATION IN BELL-JAR APPARATUS

(b) No discharge. Filament: tantalum ribbon, 5.1 by 0.36 by 0.005 centimeter

Mercury flow, ma	Length of run, hr	Initial attrition rate, k_0, cm/hr	Filament temperature, ^{o}K	Radiated power density, w/sq cm	Bell-jar pressure, mm Hg
320	55	0.38×10^{-5}	2340	45	2.0×10^{-6}
160	[a]47.5	3.9×10^{-5}	2340	45	9.0×10^{-6}
	[b]29	.51	2330	44	1.7
	101	.05	2340	45	.8
80	46	0.28×10^{-5}	2340	45	0.9×10^{-6}
	105	.50	2330	44	1.0
0	15	2.3×10^{-5}	2340	45	3.5×10^{-6}
	40	.4	↓	↓	.6
	73	.62			2.0
	128	.22	↓	↓	1.3
	60	.65	2350	46	.8

[a]Burnout.

TABLE IV. - EXPERIMENTAL DATA FOR OPERATION OF EVAPORATION TEST APPARATUS IN BELL JAR

[No mercury flow.]

Length of run, hr	Initial attrition rate, k_0, cm/hr	Filament temperature, °K	Radiated power density, w/sq cm	Bell-jar pressure, mm Hg
324	0.026×10^{-5}	2200	34	1.6×10^{-6}
291	.04	2200	34	.7
29	.56	2350	46	1.7
141	.13	2340	45	1.3
105	.44	2340	45	1.0
138	.49	2340	45	.9
129	.10	2350	46	.9
46	.30	2340	45	.9
230	.12	2340	46	.7
64	.16	2350	46	.6
44	.14	2350	46	.4
27	.07	2350	46	.2
84	.15	2370	48	1.0
[a]598	.048	2370	48	.6
[a]710	.068	2370	48	.8
[a]136	.2	2470	59	.7

[a]Burnout.

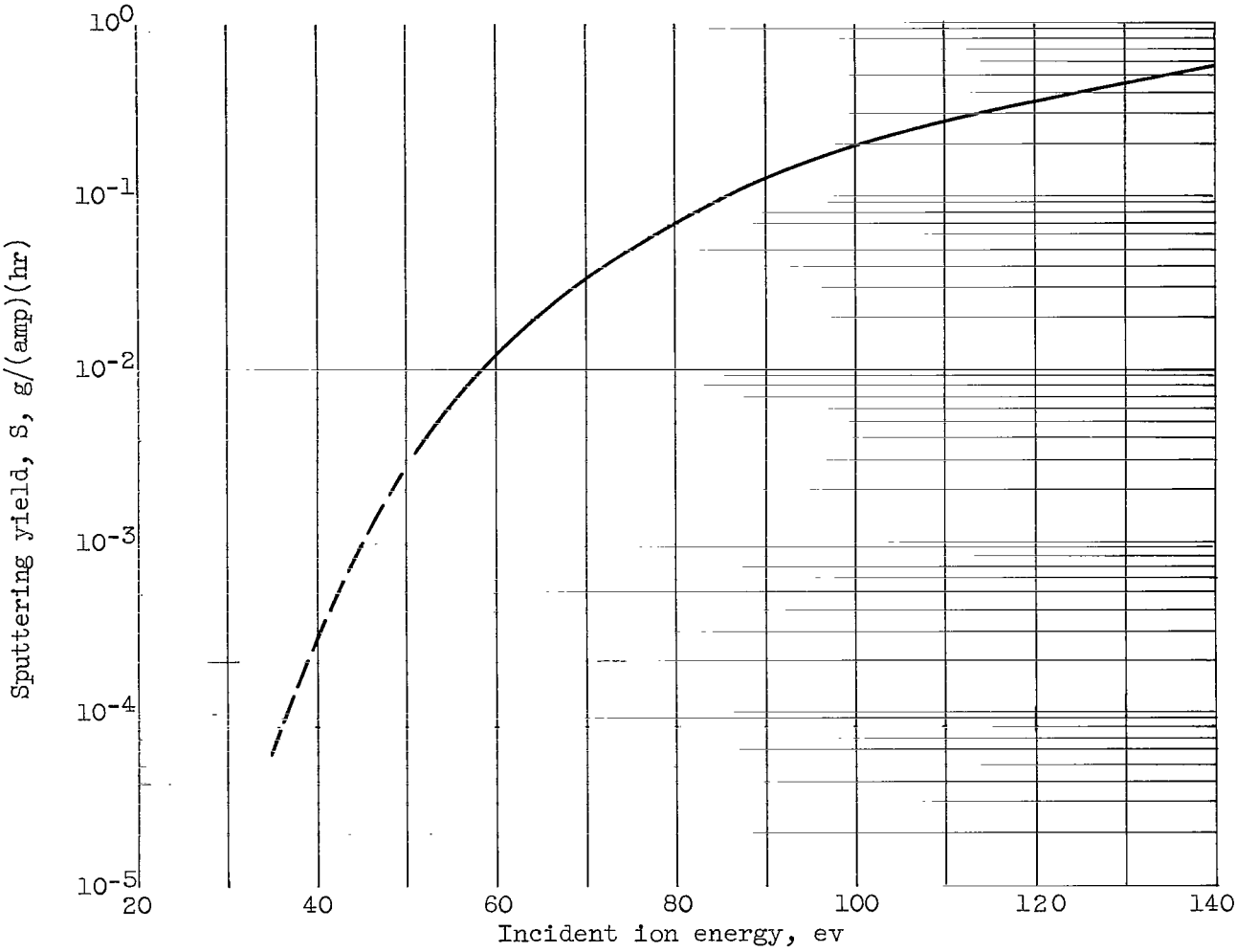

Figure 1. - Sputtering yield of mercury ions normally incident on polycrystalline tungsten (data from ref. 11).

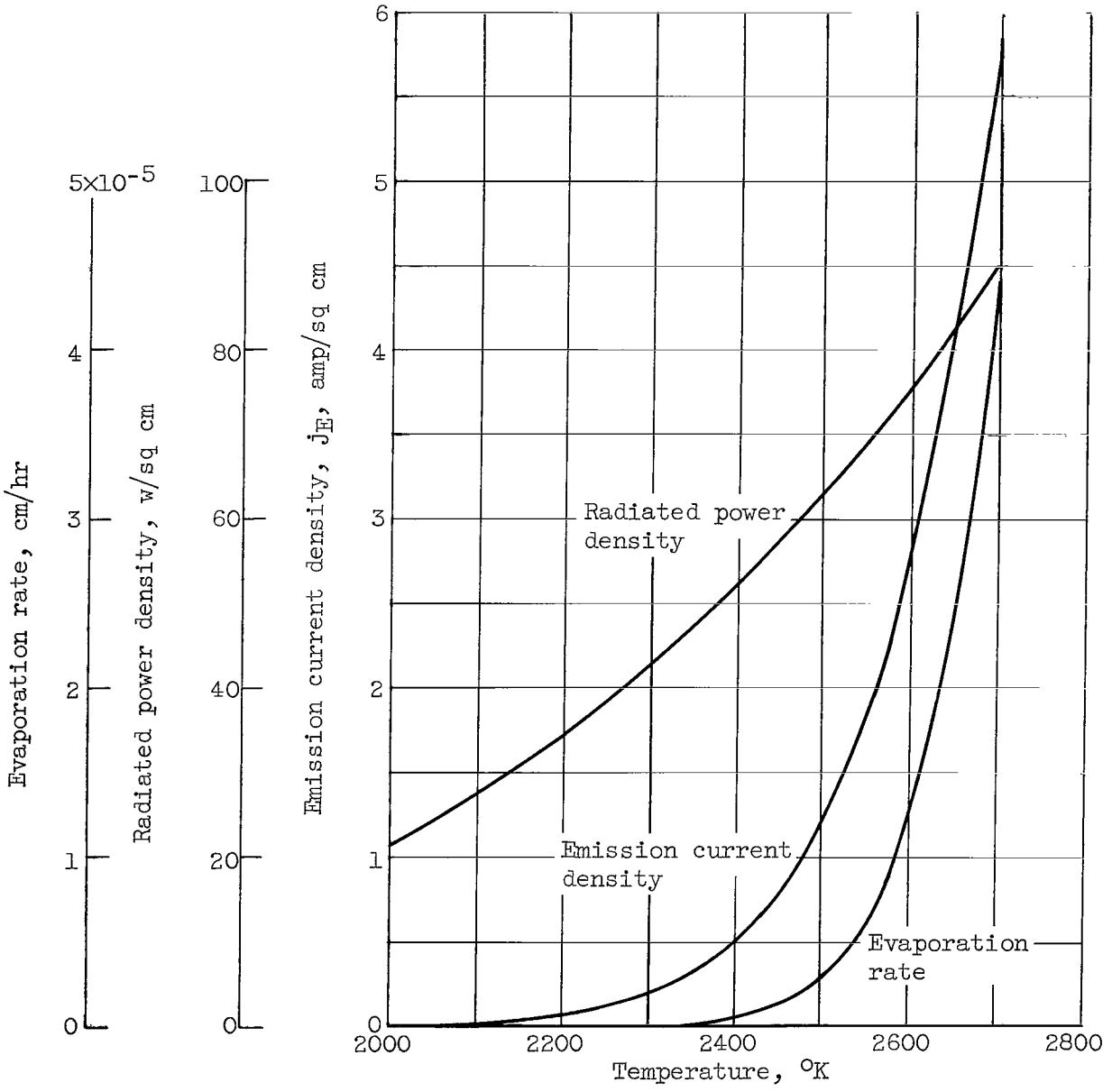

Figure 2. - Thermal characteristics of tantalum (data from ref. 7).

Figure 3. - Overall view of installation of 7.5-centimeter-diameter ion source in bell jar.

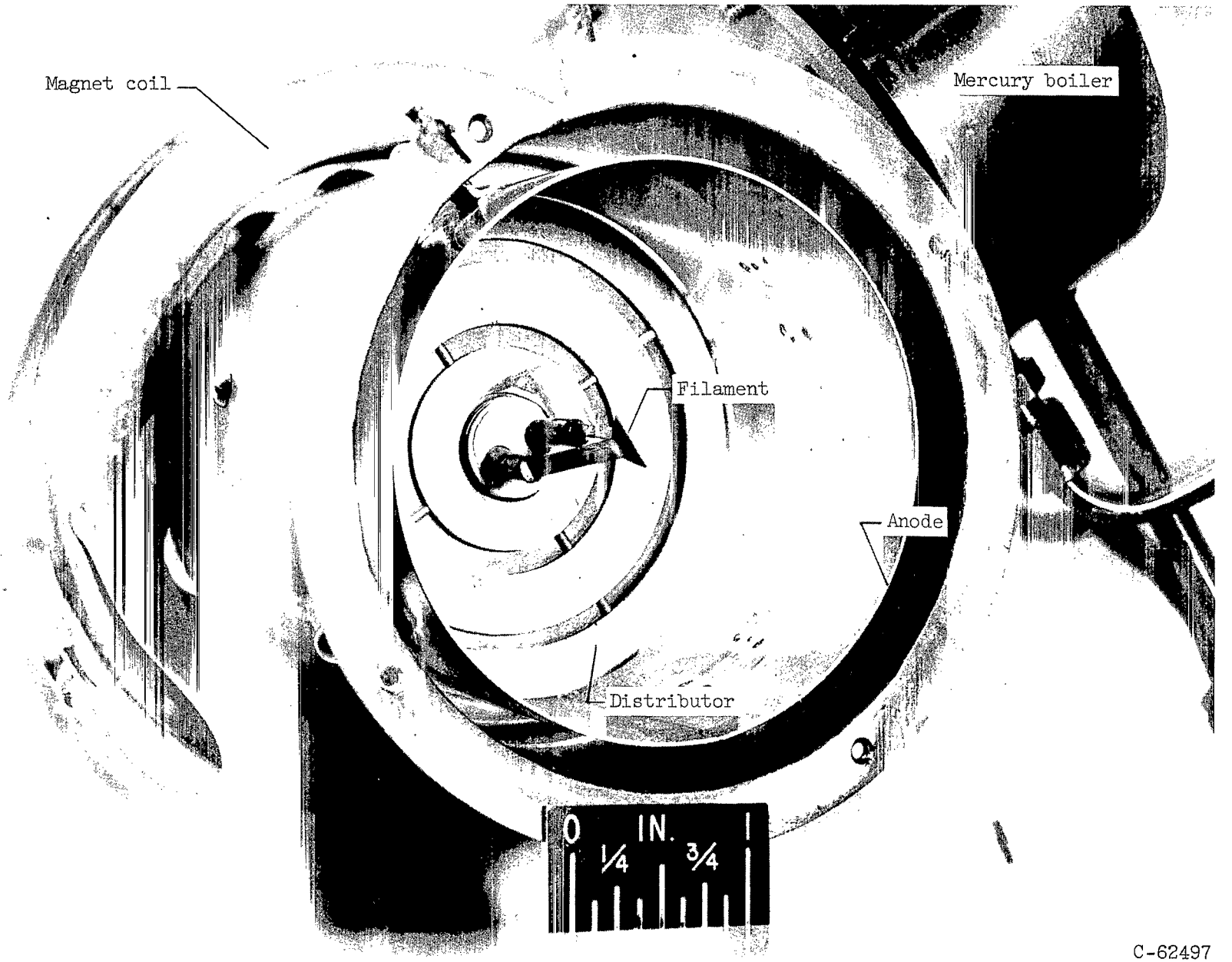

Figure 4. - Bell-jar ion source.

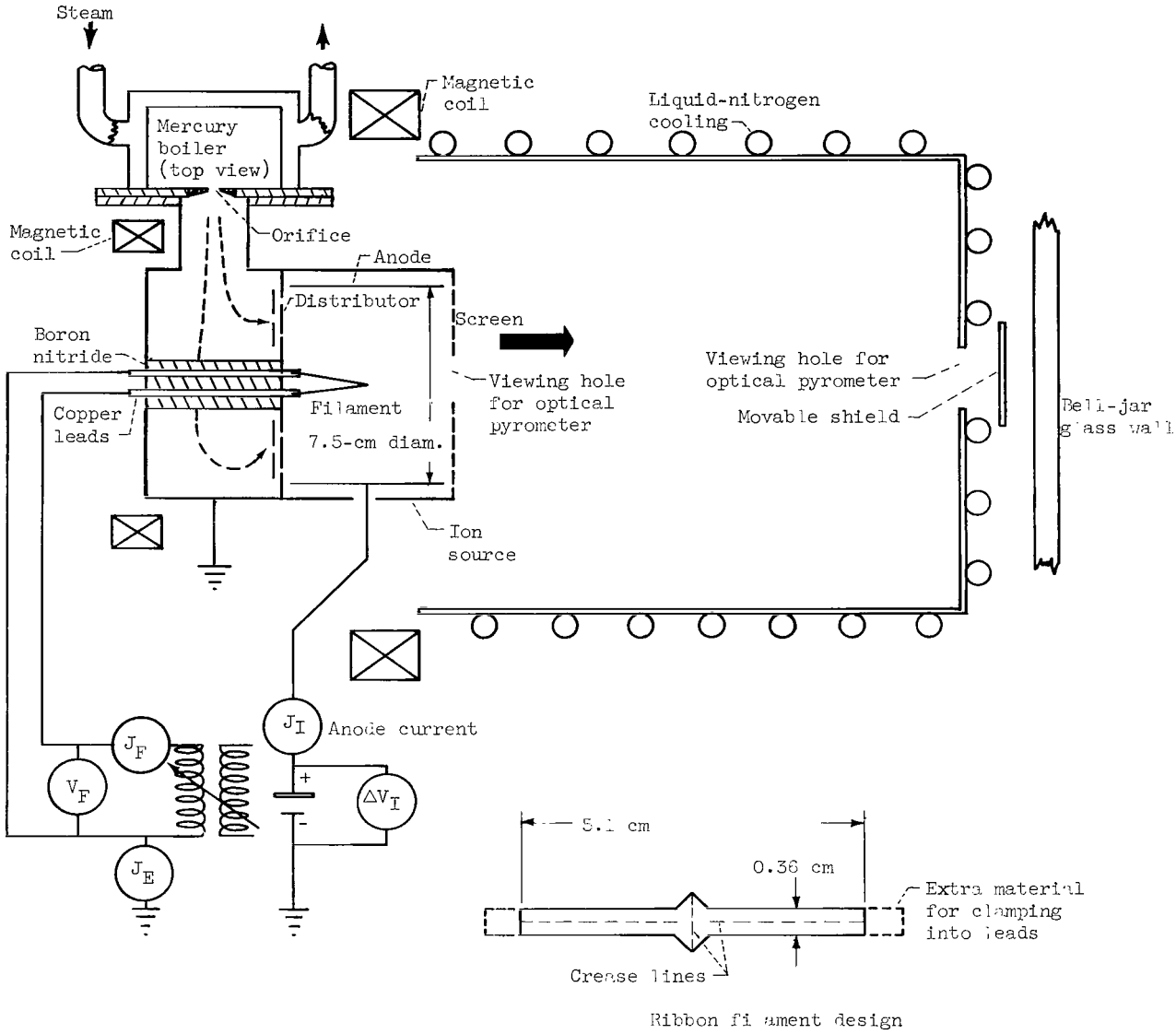

Figure 5. - Schematic diagram of electron-bombardment ion source operated in 20-inch-diameter bell jar.

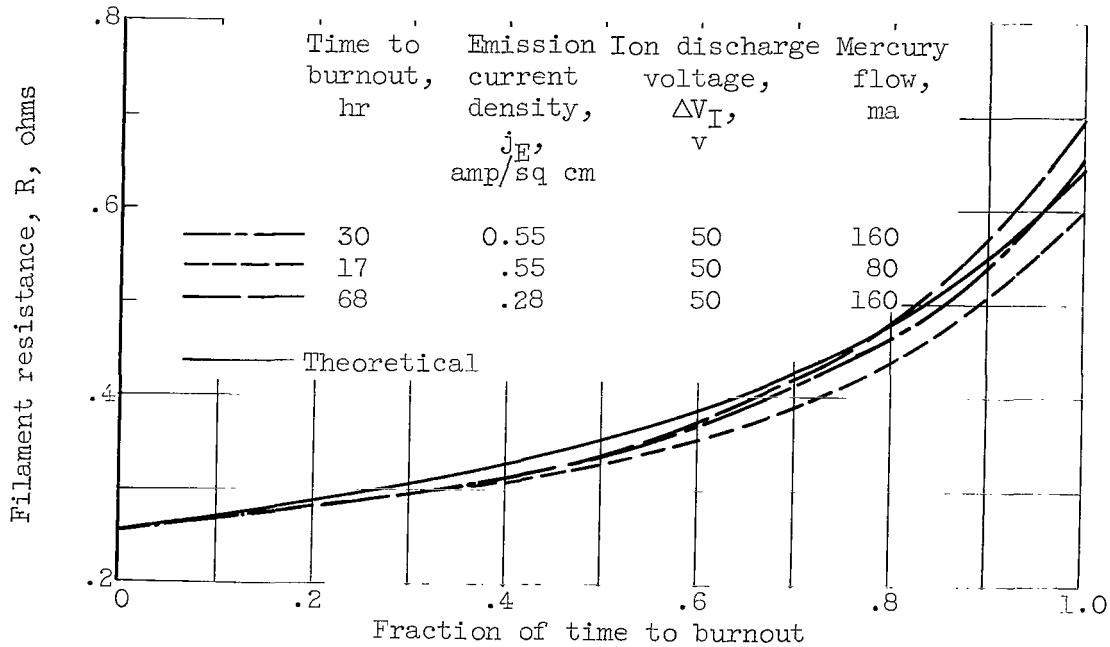

Figure 6. - Comparison of theoretical and experimental resistance of tantalum ribbon filaments. Initial thickness of ribbon, 0.005 centimeter.

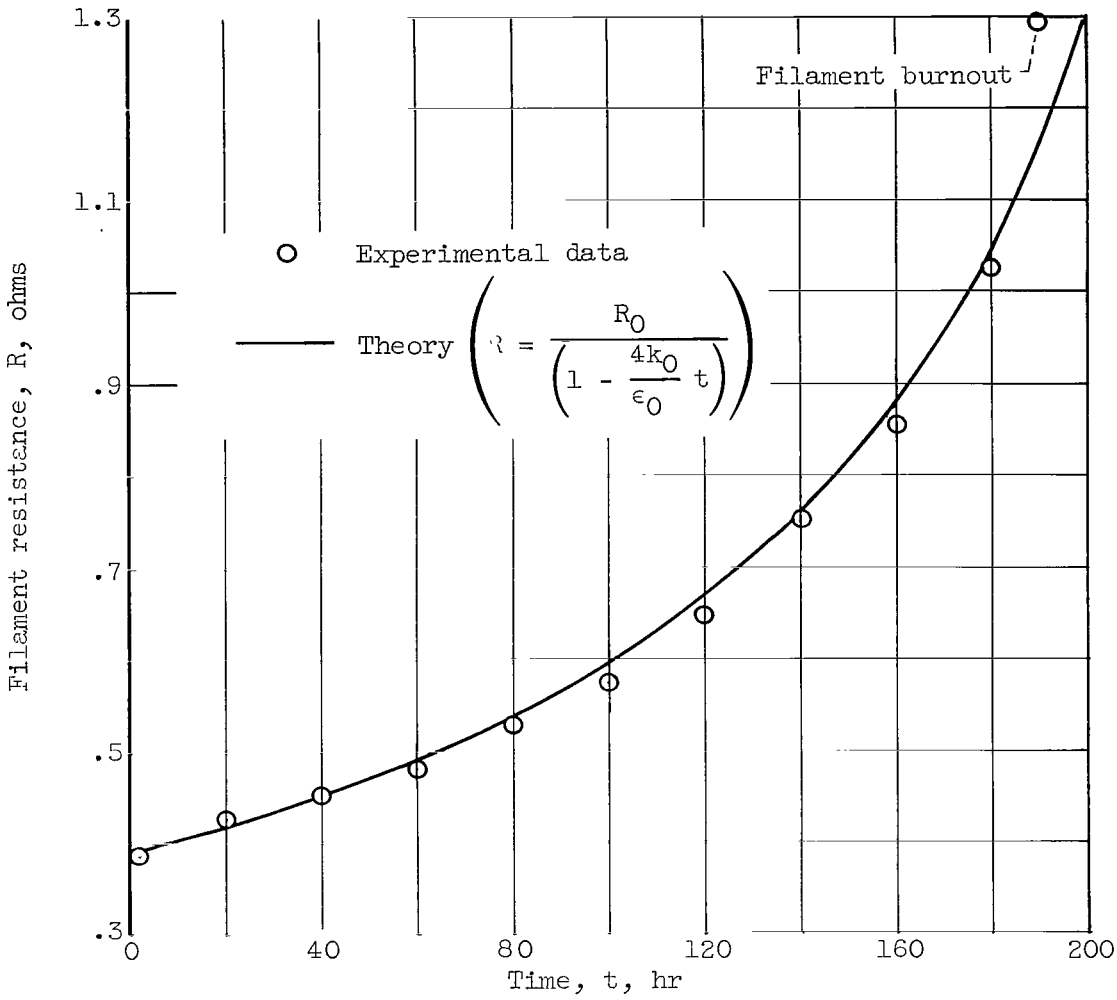

Figure 7. - Typical time variation of resistance of tantalum wire filament. Initial wire diameter, 0.025 centimeter; emission current density, 0.42 ampere per square centimeter; ion discharge voltage, 50 volts; mercury flow, 80 milliamperes. Initial resistance, attrition rate, and wire diameter, R_0, k_0, and ϵ_0, respectively.

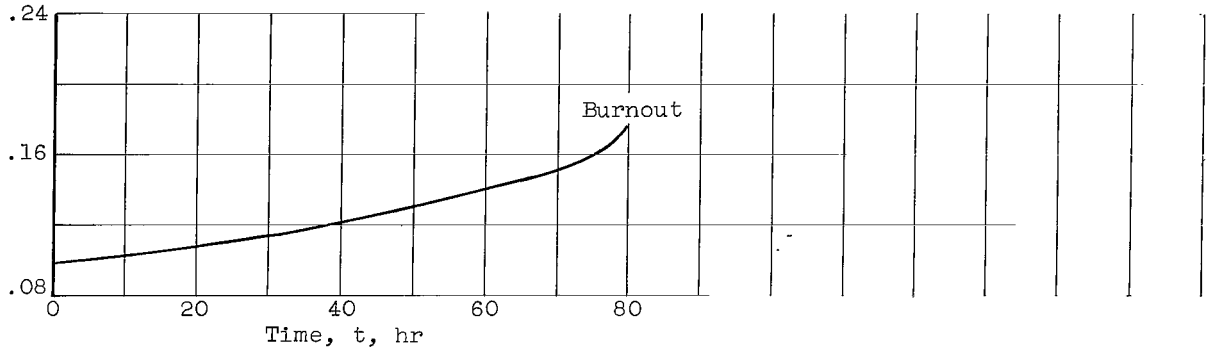

(a) Thickness of ribbon, 0.013 centimeter; emission current density, 0.55 ampere per square centimeter; ion discharge voltage, 50 volts.

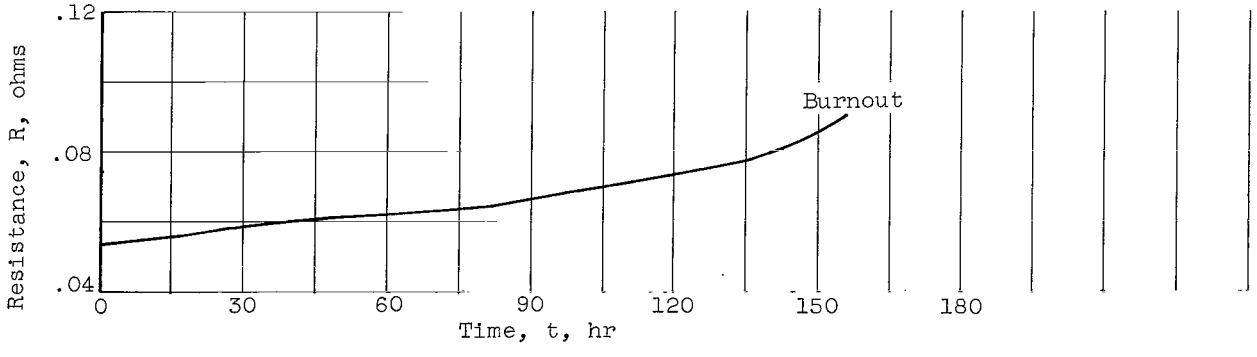

(b) Thickness of ribbon, 0.025 centimeter; emission current density, 0.55 ampere per square centimeter; ion discharge voltage, 50 volts.

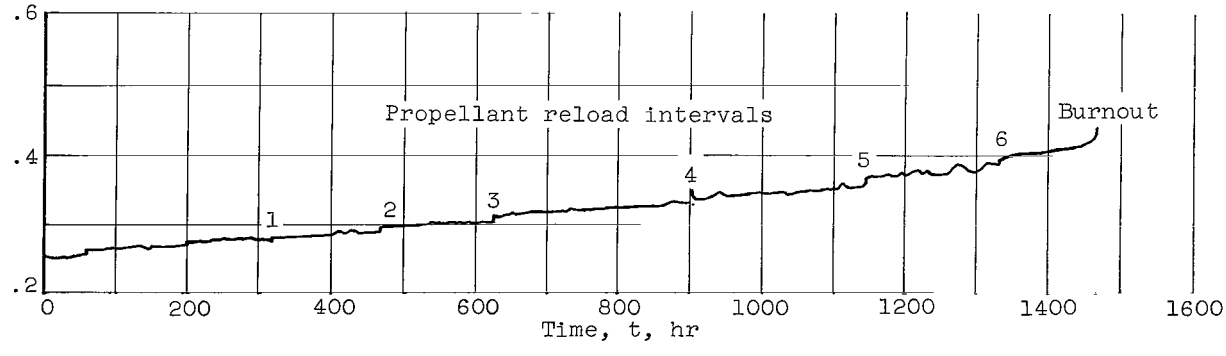

(c) Thickness of ribbon, 0.005 centimeter; emission current density, 0.14 ampere per square centimeter; ion discharge voltage, 25 volts.

Figure 8. - Time variation of resistance of tantalum ribbon filaments operating in bell-jar ion source. Mercury flow rate, 160 milliamperes.

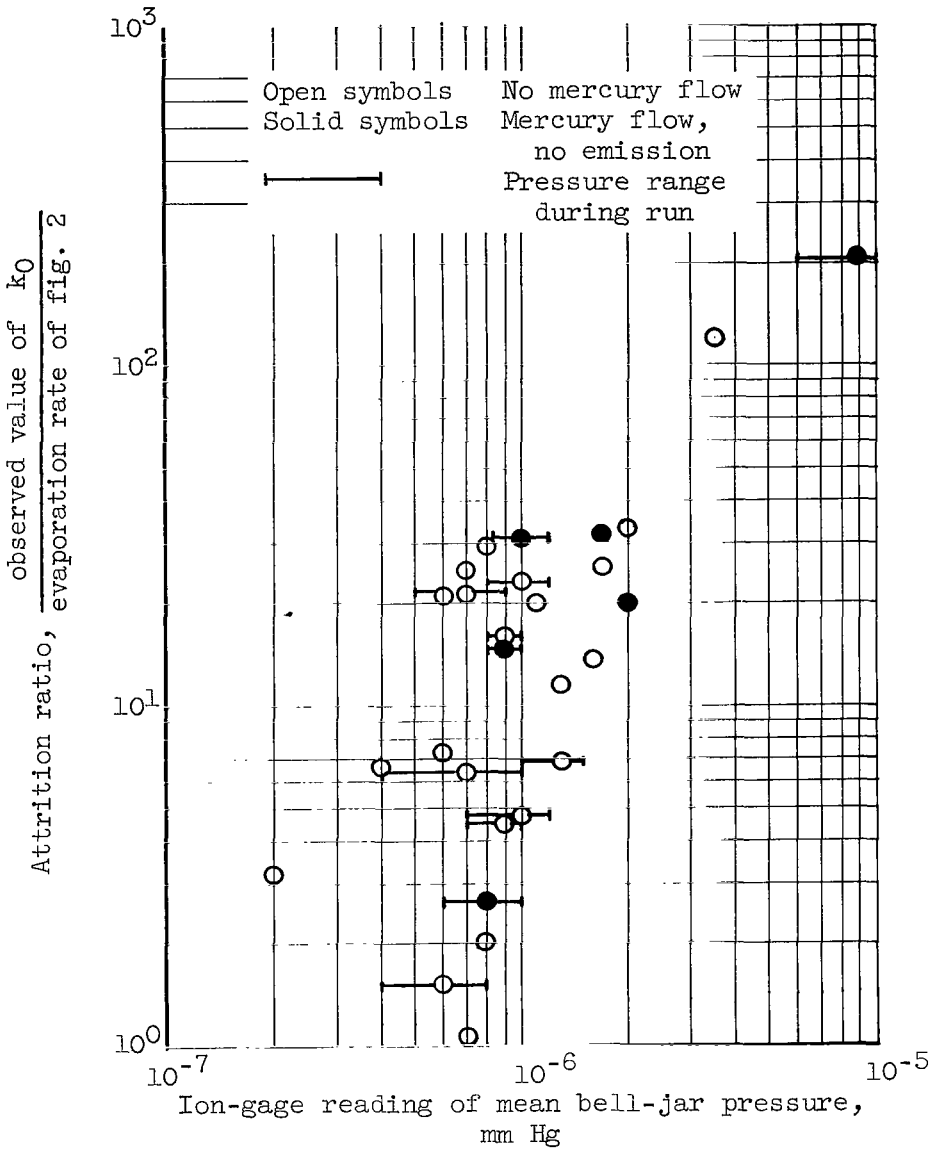

Figure 9. - Ratio of measured attrition rate to evaporation rate in vacuum as function of bell-jar pressure for tantalum ribbon filaments. Initial ribbon thickness, 0.005 centimeter.

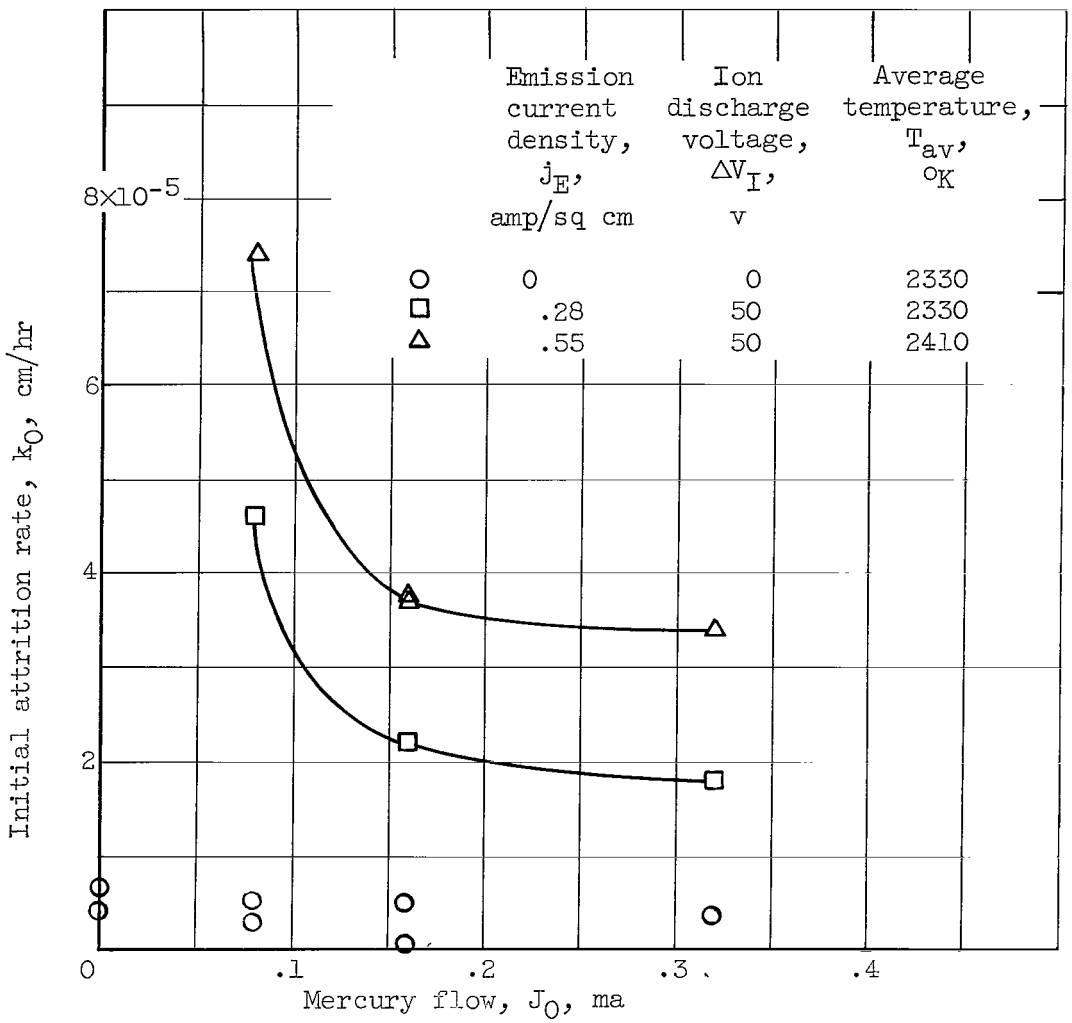

Figure 10. - Attrition rate as function of mercury flow for tantalum ribbon filaments. Ribbon dimensions, 5.1 by 0.36 by 0.005 centimeter.

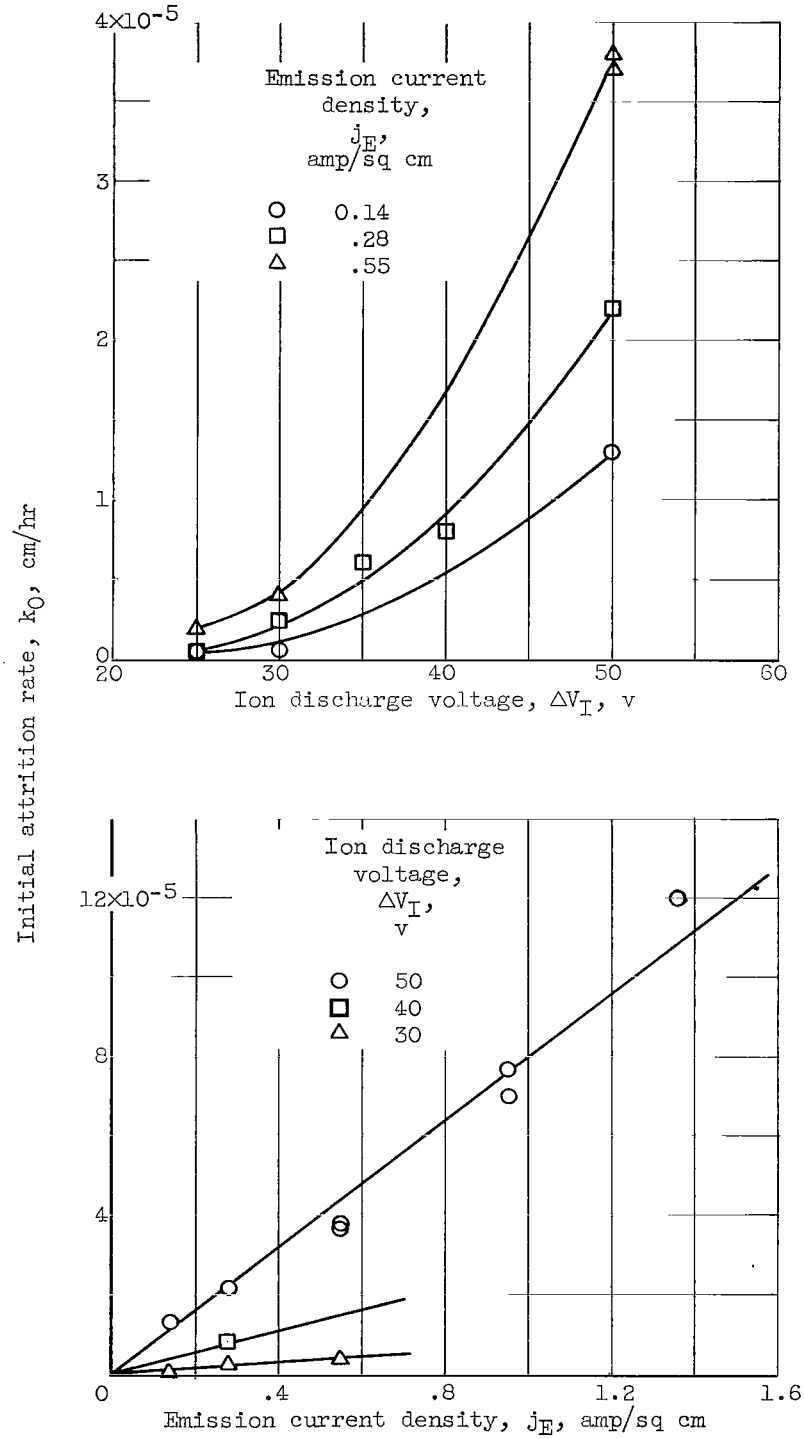

Figure 11. - Attrition rate as function of discharge voltage and emission current density for tantalum ribbon filaments. Initial ribbon thickness, 0.005 centimeter. Mercury flow, 160 milliamperes.

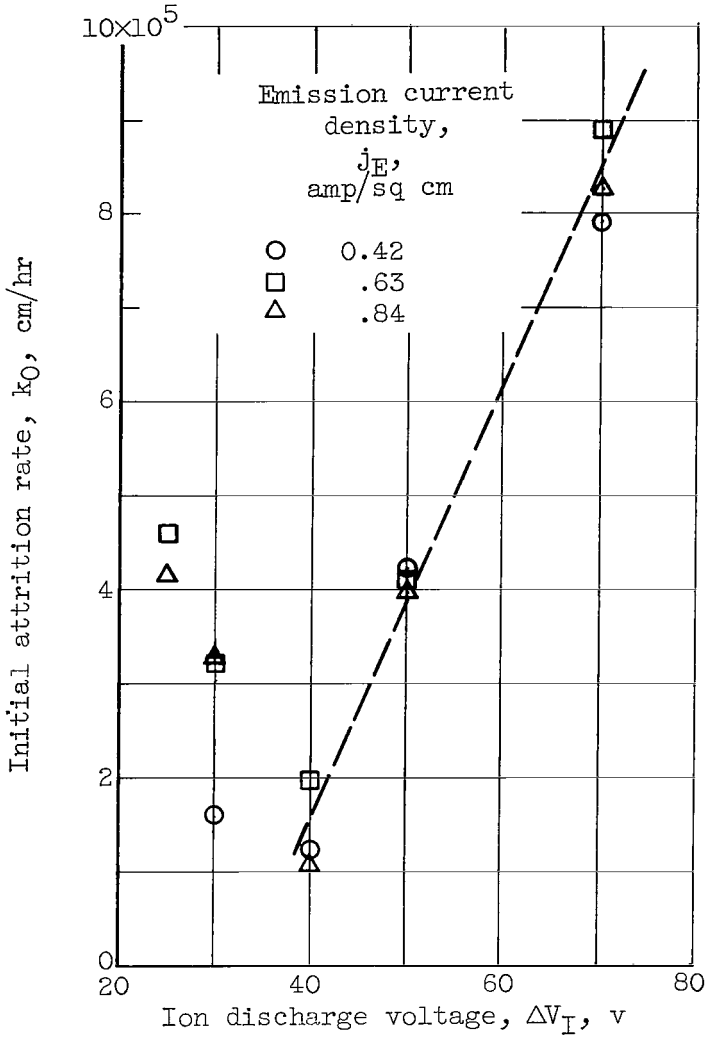

Figure 12. - Attrition rate as function of discharge voltage for tantalum wire filaments. Wire diameter, 0.025 centimeter.

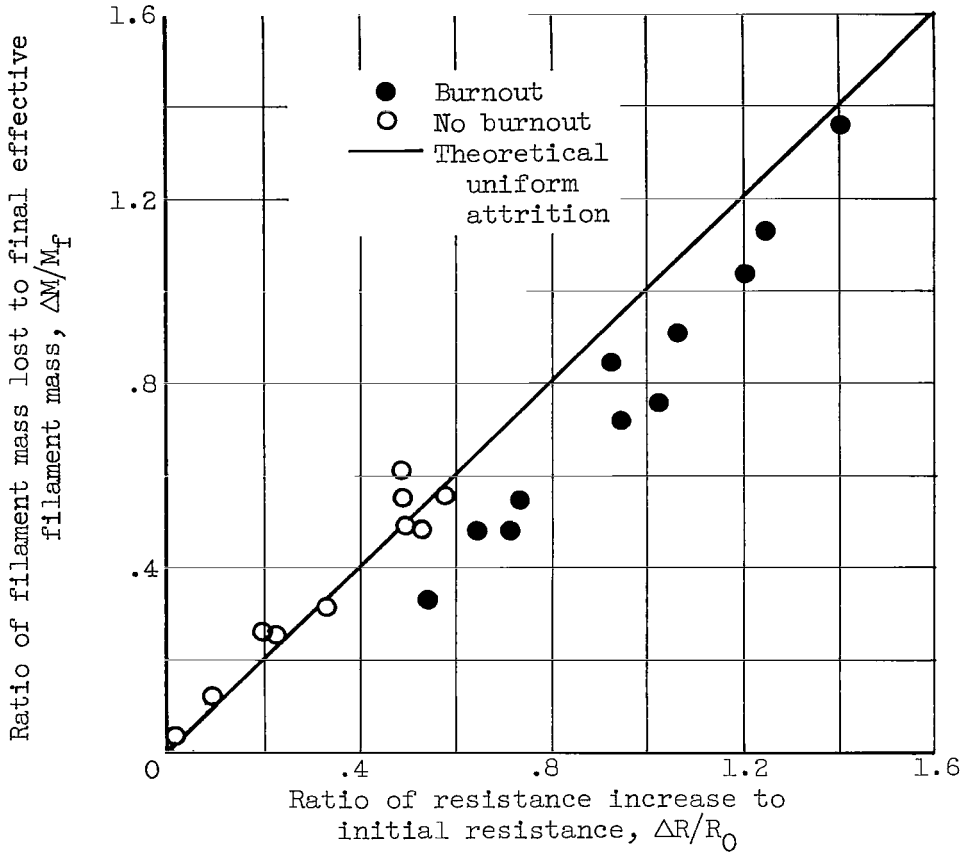

Figure 13. --Comparison of theoretical and observed uniformity of filament mass loss for tantalum ribbon filaments. Initial ribbon thickness, 0.005 centimeter.

Side of filament, X10

Burnout area

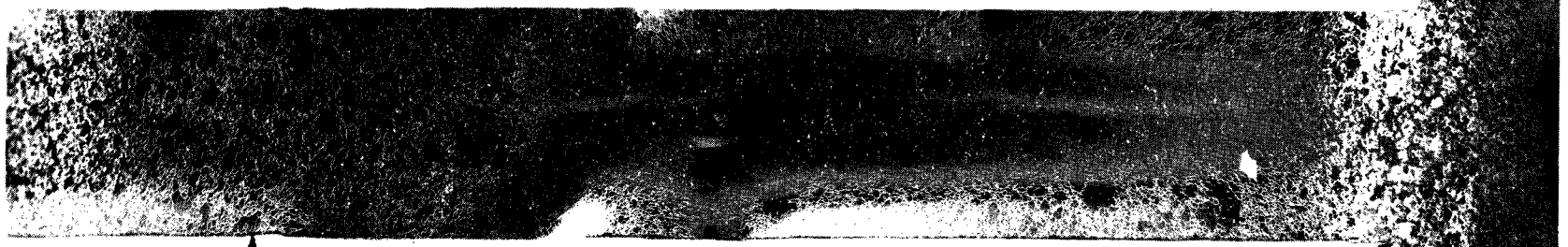

Side of filament, X10 (run stopped before burnout occurred)

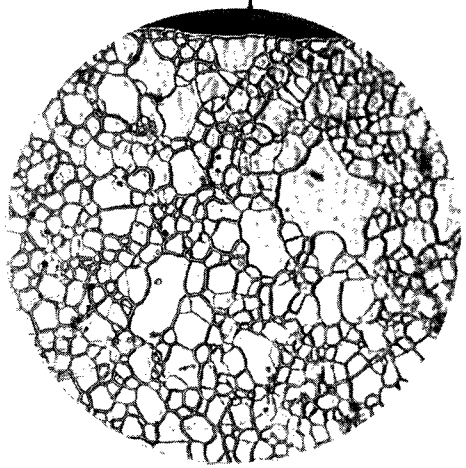

Typical grain etching, X100

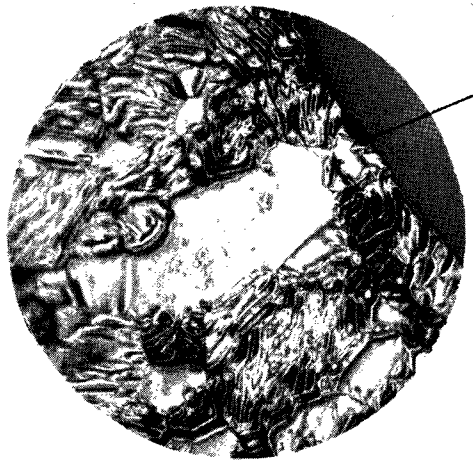

Area of higher temperature, X100

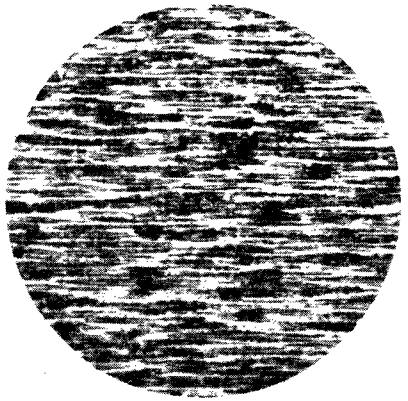

New surface, X100

C-67178

Figure 14. - Photomicrographs of tantalum ribbon filaments before and after runs. Initial ribbon thickness, 0.005 centimeter.

"The National Aeronautics and Space Administration . . . shall . . . provide for the widest practical appropriate dissemination of information concerning its activities and the results thereof . . . objectives being the expansion of human knowledge of phenomena in the atmosphere and space."

—National Aeronautics and Space Act of 1958

NASA SCIENTIFIC AND TECHNICAL PUBLICATIONS

TECHNICAL REPORTS: Scientific and technical information considered important, complete, and a lasting contribution to existing knowledge.

TECHNICAL NOTES: Information less broad in scope but nevertheless of importance as a contribution to existing knowledge.

TECHNICAL MEMORANDUMS: Information receiving limited distribution because of preliminary data, security classification, or other reasons.

CONTRACTOR REPORTS: Technical information generated in connection with a NASA contract or grant and released under NASA auspices.

TECHNICAL TRANSLATIONS: Information published in a foreign language considered to merit NASA distribution in English.

TECHNICAL REPRINTS: Information derived from NASA activities and initially published in the form of journal articles or meeting papers.

SPECIAL PUBLICATIONS: Information derived from or of value to NASA activities but not necessarily reporting the results of individual NASA-programmed scientific efforts. Publications include conference proceedings, monographs, data compilations, handbooks, sourcebooks, and special bibliographies.

Details on the availability of these publications may be obtained from:

SCIENTIFIC AND TECHNICAL INFORMATION DIVISION

NATIONAL AERONAUTICS AND SPACE ADMINISTRATION

Washington, D.C. 20546